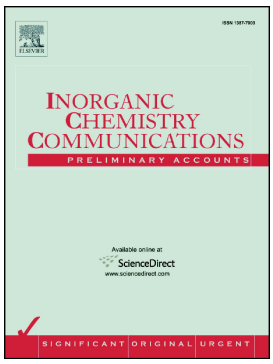

Reversible CO2 capture/release of sodium manganate with a layered structure in the presence of water vapor at 25–150 °C

Ikuo Yanase, Takano Takuya

PII: S1387-7003(18)31117-1
DOI: https://doi.org/10.1016/j.inoche.2019.01.029
Reference: INOCHE 7245

To appear in: *Inorganic Chemistry Communications*

Received date: 17 December 2018
Revised date: 17 January 2019
Accepted date: 22 January 2019

Please cite this article as: I. Yanase and T. Takuya, Reversible CO2 capture/release of sodium manganate with a layered structure in the presence of water vapor at 25–150 °C, Inorganic Chemistry Communications, https://doi.org/10.1016/j.inoche.2019.01.029

Reversible CO_2 capture/release of sodium manganate with a layered structure in the presence of water vapor at 25-150℃

Ikuo Yanase*, Takano Takuya

Saitama University, Faculty of Engineering, Department of Applied Chemistry, 255 Shimoohkubo, Sakura-ku, Saitama-shi, Saitama, 338-8570 Japan

*Corresponding Author

Tel/Fax: +81-48-858-3720

yanase@apc.saitama-u.ac.jp

Abstract

Sodium manganates with a layered structure, $Na_{0.7}MnO_{2.05}$, have been applied to a novel material for CCUS (CO_2 capture, utilization, and storage), capable of capturing CO_2 at 25 ℃ in the presence of water vapor and releasing CO_2 at 150 ℃. The temperatures of capturing and releasing CO_2 of $Na_{0.7}MnO_{2.05}$ were remarkably lower than those of other traditional metal oxides. The CO_2 absorption and desorption properties of $Na_{0.7}MnO_{2.05}$ were investigated by various methods, such as thermogravimetry, Fourier transform infrared spectroscopy, X-ray diffractometry, and gas chromatography. These investigations confirmed that $Na_{0.7}MnO_{2.05}$ absorbed CO_2 at 25 ℃ in the presence of water vapor to produce $NaHCO_3$ and a birnessite and the CO_2 absorption was promoted by increasing relative humidity and CO_2 concentration. The CO_2 absorption at 25 ℃ of $Na_{0.7}MnO_{2.05}$ was promoted by the formation of a strong basic solution on $Na_{0.7}MnO_{2.05}$, caused by the elution of Na ions from the interlayer of $Na_{0.7}MnO_{2.05}$ into water, adsorbed on the $Na_{0.7}MnO_{2.05}$ surface. Furthermore, $Na_{0.7}MnO_{2.05}$ was regenerated by heating the CO_2-absorbed $Na_{0.7}MnO_{2.05}$ at temperatures as low as 150 °C. The low-temperature regeneration indicates that $Na_{0.7}MnO_{2.05}$ can be a low-energy consumption material for capturing and releasing CO_2 at low temperatures.

Keywords: carbon dioxide; sodium manganate; water vapor; ambient temperature.

1. Introduction

Recently, inorganic materials capable of capturing and releasing CO_2 at low temperatures have been noted from the viewpoint of suppression of energy consumption in CCUS (CO_2 capture, utilization, and storage). However, various inorganic metal oxides, such as lithium silicate [1-4] and lithium ferrite [5-8] are mainly used for CO_2 captures under moderate and high temperatures and they are not appropriate for capturing and releasing CO_2 at low temperatures, except for amine-induced inorganic compounds [9,10] and metal oxides including alkaline ions [11,12].

On the other hand, it has been reported that water vapor in a CO_2 gas was effective for capturing CO_2 at low temperatures of Li_4SiO_4 and Li_2SiO_3 [13]. Furthermore, O3-$LiFeO_2$, [14-15] absorbs CO_2 from the air to produce carbonates [11] and α-$NaFeO_2$ [17-19] absorbs CO_2 from air including water vapor at low temperatures. The CO_2 absorption under water vapor at low temperatures such as 25 ℃ was promoted by an alkaline solution formed on the surface of the inorganic compounds.

Inorganic compounds, such as O3-$LiFeO_2$ and $NaFeO_2$, are expected to elute Na^+ ions under water vapor at low temperatures because these compounds have alkaline ions in the interlayer [19]. However, the above compounds are needed to release CO_2 at high temperatures after they absorbed CO_2. Therefore, it is important to develop metal oxides with a layered

structure, having low regeneration-temperatures. In this study, we focused on the layered structure of sodium manganates, $Na_{0.70}MnO_{2.05}$, having Na^+ ions in the interlayer. Hence, we examined the CO_2 absorption of the synthesized $Na_{0.7}MnO_{2.05}$ powder at 25 ℃ under a CO_2 gas flow in the presence of water vapor and its CO_2 desorption at low temperatures.

2. Experimental

Commercially available MnO_2 (>99% purity, Wako) and Na_2CO_3 (>99% purity, Wako) powders were mixed in ion-exchanged water for 1 h by an ultrasonic treatment. After removing the water with an evaporator, the mixed powder was dried and then heated at 850 °C for 5 h in air, following by cooling from 500 ℃ to room temperature (RT) under an Ar gas flow to synthesize $Na_{0.7}MnO_{2.05}$ powders.

The CO_2 absorption of the synthesized $Na_{0.7}MnO_{2.05}$ powder was carried out in a mullite tube at 25 ℃ for 5 h under a gas flow with various CO_2 concentrations. Where, the CO_2 concentration was controlled by mixing Ar gas and the gas pressure was 0.1 MPa. The relative humidity (RH) in the gas was controlled by bubbling the gases into water at 25 ℃. Both the thermal decomposition behaviors under an Ar gas flow and the CO_2 uptake behaviors of the CO_2-absorbed $Na_{0.7}MnO_{2.05}$ powders were investigated by thermogravimetry and differential thermal analysis (TG-DTA; Thermoplus TG8120, Rigaku). Furthermore, the CO_2 and H_2O

released amounts of the $Na_{0.7}MnO_{2.05}$ powders after the CO_2 absorption in the presence of water vapor were investigated by gas chromatography attached to an electrical furnace.

The produced phases were investigated by X-ray diffractometry (XRD; D8Advance, BrukerAXS) in the temperature range of 25 – 200 ℃ and Fourier transform infrared spectroscopy (FTIR; FT/IR4200, Jasco) with a KBr method. The powder morphologies of the $Na_{0.7}MnO_{2.05}$ powder before and after CO_2 absorption were examined with a field-emission scanning electron microscope (FESEM, S4100, Hitachi). The N_2 adsorption/desorption isotherms at −196 °C, examined by Belsorp-mini II (MicrotracBEL), were used to determine the Brunauer–Emmett–Teller (BET) specific surface area. The concentrations of Na^+ ions in water were measured with a Na^+ ion meter (Horiba, LAQUA B-722) and a pH meter (Horiba, LAQUA twin).

3. Results and discussion

3.1 CO_2 absorption of $Na_{0.7}MnO_{2.05}$

The XRD patterns of as-synthesized NMO and NMO absorbed CO_2 at 25 ℃ for 5 h at 15% and 75% in relative humidity (hereafter, 15% RH and 75% RH) are shown in **Fig. 1(a)** and **(b)**, respectively. At 15% RH, the NMO phase only existed and birnessite and carbonates were not produced. Conversely, at 75% RH, the NMO phase disappeared to produce birnessite

(PDF#43-1456), $NaHCO_3$ (PDF#15-0700) and $Mn_7O_{13} \cdot 5H_2O$ (PDF#23-1239) phases, indicating that the NMO reacted with CO_2 and H_2O, and the presence of water vapor promoted the reaction of NMO and CO_2. **Fig. 2** shows the results of pH testing of NMO with pH test paper in a tube furnace, under an air flow in the presence of water vapor (75% RH) at 25 ℃. The color of the pH paper changed to yellowish green (the pH changed to 9–10), indicating the production of a basic solution on the surface of the NMO particles in the presence of water vapor. Where, the CO_2 absorption of NMO set on an Al_2O_3 boat, was also performed at 25 ℃ under a CO_2 flow in the same tube furnace. A commercial $CaCl_2$ powder was used instead of water in the flask (**Fig. 2**) to prepare CO_2 gas with 15% RH. Conversely, CO_2 gas with 75% RH was prepared by bubbling a dry CO_2 gas into water.

To investigate the solubility of NMO in water, 0.14 g of NMO was dispersed into 100 ml of distilled water to prepare an NMO slurry. The result is shown in **Fig. 3(a)**. The Na^+ ion concentration and pH of the NMO slurry rapidly increased for a short time and then gradually increased to approximately 120 ppm, which corresponds to approximately 50% of the maximum Na-dissolution ratio for NMO (the theoretical concentration is 218 ppm when all Na^+ ions are eluted from 0.14 g of NMO into 100 mL of water). This result suggests that Na^+ in the interlayer of NMO easily eluted in the presence of water, leading to the formation of a NaOH solution on the surface of the NMO particles. We investigated the phase produced by elution of Na^+ of

NMO. The result shown in **Fig. 3(b)** confirmed that NMO changed to birnessite (PDF#43-1456) including H_2O molecules and Na^+ ions in the interlayer. The amount of Na^+ ions dissolved in water means that the amount of Na^+ ions decreased from approximately 0.70 in NMO to 0.31 in birnessite. The chemical composition of Na in the birnessite was almost corresponded with the other report. [20]

Fig. 4(a) shows the mass increasing behavior of NMO at 25 ℃ under a CO_2 gas flow at 80% RH, obtained by TG. The TG curve confirmed that the mass increase of NMO was increased with increasing the holing time to approximately 3 h, and it reached an almost constant level above 3 h. In the presence of water vapor, the rate-determining process is the elution of Na^+ ions into water adsorbed on the NMO surface. NMO dissolved into water droplets to produce carbonates, according to reactions (1) and (2);

$$CO_2 + 2OH^- \rightarrow CO_3^{2-} + H_2O \quad (1)$$

$$2Na^+ + CO_3^{2-} + H_2O + CO_2 \rightarrow 2NaHCO_3 \quad (2).$$

Hence, it was considered that the CO_2 absorption of NMO at 25 ℃ in the presence of water vapor proceeded according to the primary rate reaction equation (3);

$$\mathrm{Ln}\,[\mathrm{NMO}] = -kP_{CO_2}t + A \quad (3).$$

Where, [NMO] is the remaining ratio of NMO, t; the CO_2 reaction time, k; the rate constant, $k = DS / Vh$, D; the diffuse constant, S; the surface area, V; the volume of solution, h; the

thickness of diffusion layer, P_{CO_2}; the partial pressure of CO_2, A; a constant. The parameter k refers to the Nernst-Noyes-Whitney equation for dissolution of solids [21,22]. **Fig. 3(b)** shows the relationship between the remaining ratio of NMO, [NMO] and holding time, t for the TG curves in **Fig. 3(a)**. Here, the partial pressure, P_{CO_2} = 1 atm. The result indicates that the CO_2 absorption rate of NMO was influenced by elution of Na^+ ions into water adsorbed on the NMO surface below approximately 1 h. On the other hand, the rate-determining process above 1 h was the diffuse reaction of CO_2 because carbonates and a birnessite increased on the surface as the CO_2 absorption proceeded.

The morphologies of the as-synthesized NMO and NMO absorbed CO_2 at 25 ℃ for 5 h under a CO_2 flow at 75% RH, are shown in **Figs. 5(a)** and **(b)**, respectively. Compared to the as-synthesized NMO, small particles of $NaHCO_3$ were observed on the surface of the CO_2-absorbed NMO, which was formed during CO_2 absorption under water vapor. The CO_2 absorption of NMO at 25 ℃ under water vapor occurred according to the schematic of **Fig. 5(c)**. Thus, a basic solution formed on the surface of NMO, owing to Na^+ elution from the layered structure of NMO, which promoted the reaction of CO_2 and NMO, resulting in production of birnessite and $NaHCO_3$. The XRD patterns and FTIR spectra of the NMO powder absorbed CO_2 with concentrations of 20%, 50% and 100% under 75% RH, together with the as-synthesized NMO powder are shown in **Figs. 6(a)** and **(b)**, respectively. The XRD patterns show that the

NMO phase decreased and the birnessite phase increased as the CO_2 concentration increased from 20% to 100%. The FTIR spectra confirmed that the largest absorption peaks at around 1350 cm^{-1} of $NaHCO_3$ and those at around 1400 cm^{-1} of $Na_2CO_3 \cdot H_2O$ were assigned to asymmetric vibrations of HCO_3^- and CO_3^{2-}, respectively [23,24] and $NaHCO_3$ was clearly produced at 50% and 100%-CO_2 concentrations.

3.2 Decomposition of CO_2-absorbed $Na_{0.7}MnO_{2.05}$

The TG (a) and DTA (b) curves of NMO absorbed CO_2 at concentrations from 20% to 100% at 25 ℃ for 5 h in the presence of water vapor are shown in **Fig. 7**. The mass decrease rates for CO_2-absorbed NMO increased as the CO_2 concentration increased. The mass decrease was mainly caused by decomposition of $NaHCO_3$. The endothermic peaks for CO_2-absorbed NMO were mainly observed at temperatures below 90 °C for the case of 20%-CO_2 concentration. This result indicates that production of $NaHCO_3$ requires a higher CO_2 concentration because $NaHCO_3$ was not produced at a CO_2 concentration of 20%, as shown in **Fig. 6**. The CO_2 and H_2O absorption amounts of the CO_2-absorbed NMO was investigated. The results are shown in **Fig. 7(c)** and **(d)**. The absorption of CO_2 for was greater than that of H_2O, indicating that NMO absorbed CO_2 together with H_2O and Na^+ ions in the interlayer was effective for absorbing CO_2 at 25 ℃ in the presence of water vapor.

3.3 Regeneration of $Na_{0.7}MnO_{2.05}$

The high-temperature XRD patterns of the powders obtained by heating the CO_2-absorbed NMO at temperatures from 25 ℃ to 200 °C in air are shown in **Fig. 8**. The birnessite phase decreased and the NMO phase increased at 100 °C, although the birnessite phase was identified at 50 °C. The birnessite phase disappeared and the NMO phase only appeared at 150 °C. Thus, NMO was regenerated at temperatures as low as 150 °C, which is considerably lower than the regeneration temperatures of other CO_2-absorbing materials containing alkaline ions, such as 700 °C for Li_4SiO_4 [1,13], 500 °C for $LiFeO_2$ [6,7]. We attribute the low-temperature regeneration of NMO to the low-temperature reactions of birnessite and $NaHCO_3$. The low-temperature regeneration indicates that the Na^+ ions could be induced into the interlayer of birnessite, which have fewer Na^+ ions, by the thermal decomposition of $NaHCO_3$ to produce NMO having a layered structure containing any interlayer Na^+ ions.

SEM images and N_2 adsorption/desorption isotherms of the as-synthesized NMO and regenerated NMO powders are shown in **Fig. 9**. The SEM images showed that the regenerated NMO particles were smaller than those of the as-synthesized NMO. The N_2 adsorption/desorption isotherms confirmed that the specific surface area of the regenerated NMO (12.5 m^2/g) was much higher than that of the as-synthesized NMO (0.8 m^2/g). This is

because the small particles (**Fig. 9(b)**) on the regenerated NMO ware produced by the thermal decomposition of the small $NaHCO_3$ particles formed by the reaction of CO_2 with small NaOH droplets on the NMO surface. **Fig. 10** shows CO_2 and H_2O amounts released from the as-synthesized NMO, the regenerated NMO at the 1st cycle (hereafter, 1st-reNMO), 2nd cycle (hereafter, 2nd-reNMO), and 3rd cycle (hereafter, 3rd-reNMO). The mass ratios of CO_2 for the 1st-reNMO, 2nd-reNMO, and 3rd-reNMO were larger than that of the as-synthesized NMO. The increase of the released amounts of CO_2 and H_2O was caused by the increase of the specific surface area of the regenerated NMO, as shown in Fig. 9. Thus, the regenerated NMO is also capable of capturing and stabilizing CO_2 in the presence of water vapor.

4. Conclusion

$Na_{0.7}MnO_{2.05}$ (NMO) with a layered structure was synthesized by a solid-state reaction method. NMO absorbed CO_2 at 25 ℃ under CO_2 flows with various CO_2 concentrations in the presence of water vapor to produce $NaHCO_3$ and birnessite. The CO_2 absorption ratio at 25 ℃ of NMO increased with increasing the CO_2 concentration in the presence of water vapor. The CO_2 absorption of NMO at 25 ℃ was caused by the formation of a basic solution on the surface of NMO by adsorption of water vapor on the surface. NMO was regenerated by heating the CO_2-absorbed NMO at temperatures as low as 150 °C. The low-temperature regeneration of

NMO indicates that NMO can be used as a CO_2-capture material at 25 ℃ in the presence of water vapor.

Acknowledgments This work was supported by a Grant-in-Aid for Scientific Research (C) (18K05269) of Japan Society of the Promotion of Science (JSPS).

References

[1] K. Essaki, M. Kato, K. Nakagawa, CO_2 removal at high temperature using packed bed of lithium silicate pellets, J. Ceram. Soc. Jpn. 114 (2006) 739-742.

[2] Q. Zhang, X. Liang, D. Peng, X. Zhu, Development of a fly ash derived Li_4SiO_4-based sorbent for CO_2 capture at high temperatures, Thermochimica Acta 669 (2018) 80-87.

[3] S. Shan, Q. Jia, L. Jiang, Q. Li, Y. Wang, J. Peng, Novel Li_4SiO_4-based sorbents from diatomite for high temperature CO_2 capture, Ceramics Int. 39 (2013) 5437-5441.

[4] K. Wang, Z. Yin, P. Zhao, Synthesis of macroporous Li_4SiO_4 via a citric acid-based sol-gel route coupled with carbon coating and its CO_2 chemisorption properties, Ceramics Int. 42 (2016) 2990-2999.

[5] M. Kato, K. Essaki, K. Nakagawa, Y. Suyama, K. Terasaki, Carbonation properties of lithium ferrite for application as a high-temperature CO_2 absorbent, J. Ceram. Soc. Jpn. 113

(2005) 684-686.

[6] I. Yanase, A. Kameyama, H. Kobayashi, Carbonation and structural phase transformation of α-$LiFeO_2$, J. Ceram. Soc. Jpn. 118 (2010) 48-51.

[7] I. Yanase, H. Otsuka, H. Kobayashi, Carbonation of CeO_2-coated α-$LiFeO_2$, J. Ceram. Soc. Jpn. 119 (2011) 933-938.

[8] I. Yanase, J. Miura, H. Kobayashi, Carbonation and phase transformation of $LiMO_2$ (M=Fe, Co, Ni) under CO_2 atmosphere, Materials Chemistry and Physics 199 (2017) 18-22.

[9] Q. Lai, Z. Diao, L. Kong, H. Adidharma, M. Fan, Amine-ompregnated silicic acid composites as an efficient adsorbent for CO_2 capture, Applied Energy 223 (2018) 293-301.

[10] A. Wells, Y. Fang, L.T.-Murciano, A. Nearchou, Z. Dong, T.J. White, A. Sartbaeva, V.P. Ting, Mechanism of CO_2 capture in nanostructured sodium amide encapsulated in porous silica, Surface and Coatings Technology 350 (2018) 227-233.

[11] M.S. Cho, C. Lee, H.J. Chae, Y.M. Kwon, H.J. Kim, Y. Ryu, B. Lee, J.C. Kim, Optimum design and characteristics of potassium-based sorbents using SiO_2 for post-combustion CO_2 capture, Renewable Energy Available online, 2018.

[12] R. R.-Mosqueda, E.A. Bramer, G. Brem, CO_2 capture from ambient air using hydrated Na_2CO_3 supported on activated carbon honeycombs with application to CO_2 enrichment in greenhouses, Chemical Engineering Science 189 (2018) 114-122.

[13] J.O.-Landeros, R. L.-Juarez, I.C. R.-Ibarra, H. Pfeiffer, H.B.-Ramirez, C.G.-Yanez, Li_2SiO_3 fast microwave-assisted hydrothermal synthesis and evaluation of its water vapor and CO_2 absorption properties, Particuology 24 (2016) 129-137.

[14] M. Barre, M. Catti, Neutron diffraction study of the β' and γ phases of $LiFeO_2$, J. Solid State Chem. 182 (2009) 2549-2554.

[15] M. Tabuchi, S. Tsutsui, C. Masquelier, R. Kanno, K. Ando, I. Matsubara, S. Nasu, H. Kageyama, Effect of cations arrangement on the magnetic properties of lithium ferrites ($LiFeO_2$) prepared by hydrothermal reaction and post-annealing method, J. Solid State Chem. 140 (1998) 159-167.

[16] Y.S. Lee, S. Sato, Y.K. Sun, K. Kobayakawa, Y. Sato, A new type of orthorhombic $LiFeO_2$ with advanced battery performance and its structural change during cycling, J. Power Sources 110-121 (2003) 285-289.

[17] H. Yoshida, N. Yabuuchi, S. Komaba, $NaFe_{0.5}Co_{0.5}O_2$ as high energy and power positive electrode for Na-ion batteries, Electrochemistry Comm. 34 (2013) 60-63.

[18] P. Vassilaras, A.J. Toumar, G. Ceder, Electrochemical properties of $NaNi_{1/3}Co_{1/3}Fe_{1/3}O_2$ as a cathode material for Na-ion batteries, Electrochemistry Comm. 38 (2014) 79-81.

[19] E. Monyoncho, R. Bissessur, Unique properties of α-$NaFeO_2$: De-intercalation of sodium via hydrolysis and the intercalation of guest molecules into the extra solution, Materials

Research Bulletin 48 (2013) 2678-2686.

[20] Kh.S. A.-E.-Sherbini, M.H. Askar, R. Schollhorn, Hydrated layered manganese dioxide Part I. Synthesis and characterization of some hydrated layered manganese dioxides from α-$NaMnO_2$, Solid State Ionics 150 (2002) 407-415.

[21] J.J. L-Quintana, J.K. R.-Guerrero, P.G. Valenca, Carbonate hydroxyapatite as a catalyst for ethanol conversion to hydrocarbon fuels, Applied Catalyst A, General 542 (2017) 136-145.

[22] S. Garcia, E.S. Fernadez, A.J. Stewart, M.M. M.-Valer, Process integration of post-combustion CO_2 capture with Li_4SiO_4/Li_2CO_3 looping in a NGCC plant, Energy Procedia 114 (2017) 2611-2617.

[23] Z.S. Nickolov, O. Ozcan, J.D. Miler, FTIR analysis of water structure and its significance in the flotation of sodium carbonate and sodium bicarbonate salts, Colloids and Surfaces A: Physicochem. Eng. Aspects 224 (2003) 231-230.

[24] B. Dutcher, M. Fan, B. Leonard, M.D. Dyar, J. Tang, E.A. Speicher, P. Liu, Y. Zhang, Use of nanoporous FeOOH as a catalysis support for $NaHCO_3$ decomposition aimed at reduction of energy requirement of $Na_2CO_3/NaHCO_3$ based CO_2 separation technology, J. Phys. Chem. C 115 (2011) 15532-15544.

Figure captions

Fig. 1 XRD patterns of powders of as-synthesized NMO and CO_2-absorbed NMO under CO_2 flow at 25 ℃under (a) 15 and (b) 75% RH.

Fig. 2 Schematic showing the pH testing of NMO with pH test paper in the tube furnace, under an air flow in the presence of water vapor (75% RH) at 25 ℃.

Fig. 3 (a) Na^+ ion concentration and pH of NMO slurry prepared by dispersion of NMO into distilled water and (b) XRD pattern of dried powder obtained after measurements of Na^+ ion concentration and pH.

Fig. 4 (a) TG curve for the mass increasing behavior of NMO at 25 ℃ under a CO_2 gas flow at 80% RH. (b) Relationship between the remaining ratio of NMO, [NMO] and holding time, *t*.

Fig. 5 Powder morphologies of (a) as-synthesized NMO and (b) CO_2-absorbed NMO at 25 ℃ for 5 h under a flow of CO_2 with 75% RH. (c) Scheme for the CO_2 absorption mechanism at 25 ℃of NMO in the presence of water vapor.

Fig. 6 (a) XRD patterns and (b) FTIR spectra of the NMO powders absorbed CO_2 for 5 h at concentrations of 20%, 50% and 100% under 75% RH.

Fig. 7 (a) TG and (b) DTA curves for thermal decomposition under an Ar gas flow for NMO. CO_2 and H_2O absorption amounts of CO_2-absorbed NMO (c, d). CO_2 absorption of NMO was carried out at 25 ℃ for 5 h under 75% RH.

Fig. 8 High-temperature XRD patterns of samples powders obtained by heating the CO_2-absorbed NMO at temperatures from 25 ℃ to 200 °C in air, with a heating rate of 5 °C/min.

Fig. 9 SEM images and N_2 adsorption/desorption isotherms of as-synthesized NMO and regenerated NMO powders.

Fig. 10 CO_2 and H_2O released from as-synthesized NMO, regenerated NMO for the 1st cycle (1st-reNMO), 2nd cycle (2nd-reNMO), and 3rd cycle (3rd-reNMO). CO_2 absorption of NMO was carried out at 25 ℃ for 5 h under 75% RH.

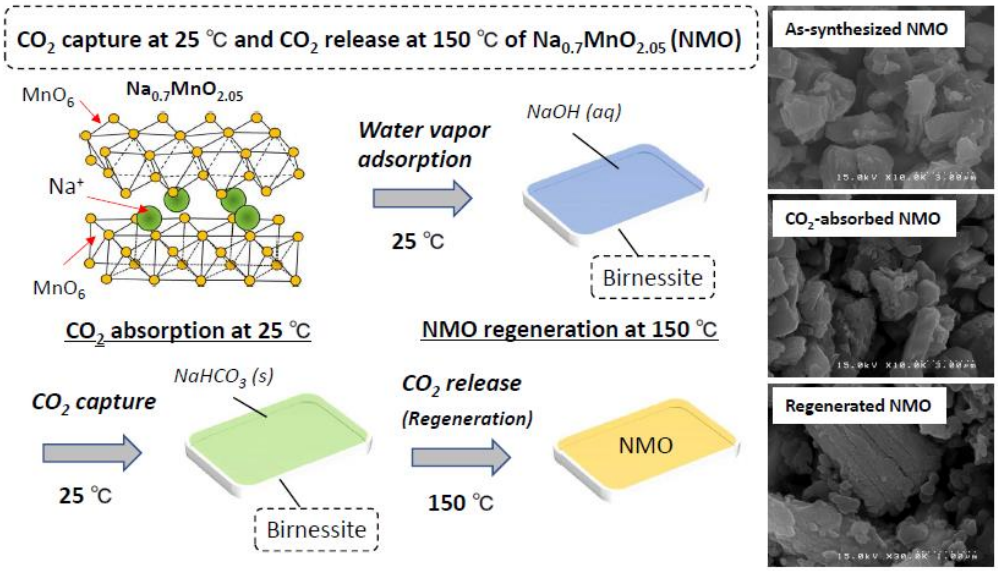

Graphical abstract

Highlights

- $Na_{0.7}MnO_{2.05}$ was applied to a novel capturing/releasing CO_2 material at low temperatures.
- The CO_2 capture of $Na_{0.7}MnO_{2.05}$ was promoted at 25 ℃ by increasing relative humidity and CO_2 concentration.
- Adsorption of water vapor on the surface of $Na_{0.7}MnO_{2.05}$ caused the low-temperature CO_2 absorption.
- $Na_{0.7}MnO_{2.05}$ was regenerated at temperatures as low as 150 °C.

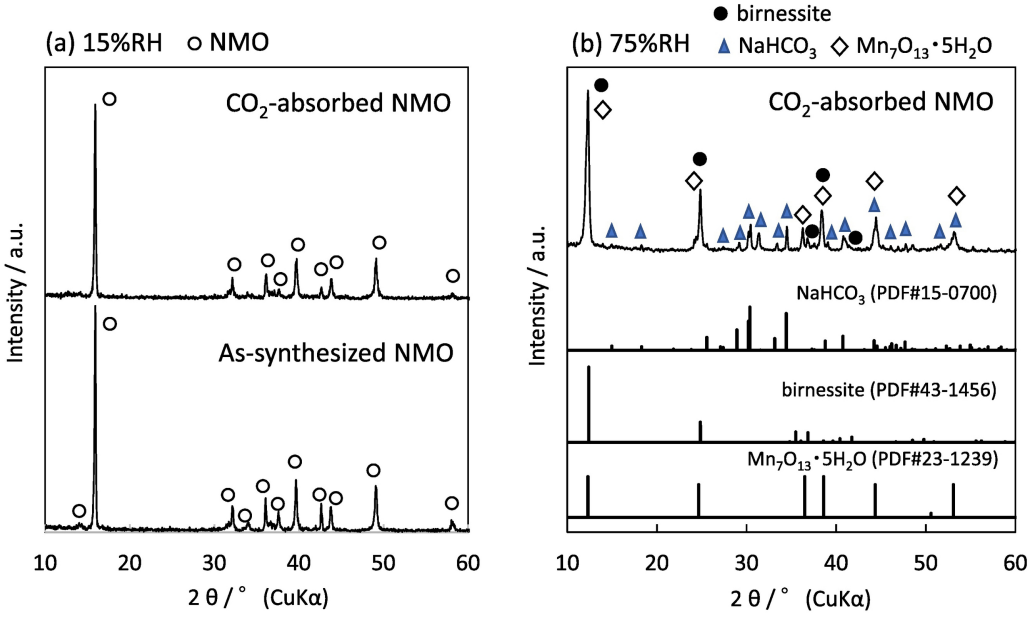
(a) 15%RH
NMO
CO2-absorbed NMO
As-synthesized NMO
Intensity / a.u.
10
20
30
40
50
60
2 θ / ° (CuKα)
birnessite
(b) 75%RH
NaHCO3
Mn7O13·5H2O
CO2-absorbed NMO
NaHCO3 (PDF#15-0700)
birnessite (PDF#43-1456)
Mn7O13·5H2O (PDF#23-1239)
Intensity / a.u.
10
20
30
40
50
60
2 θ / ° (CuKα)

Figure 1

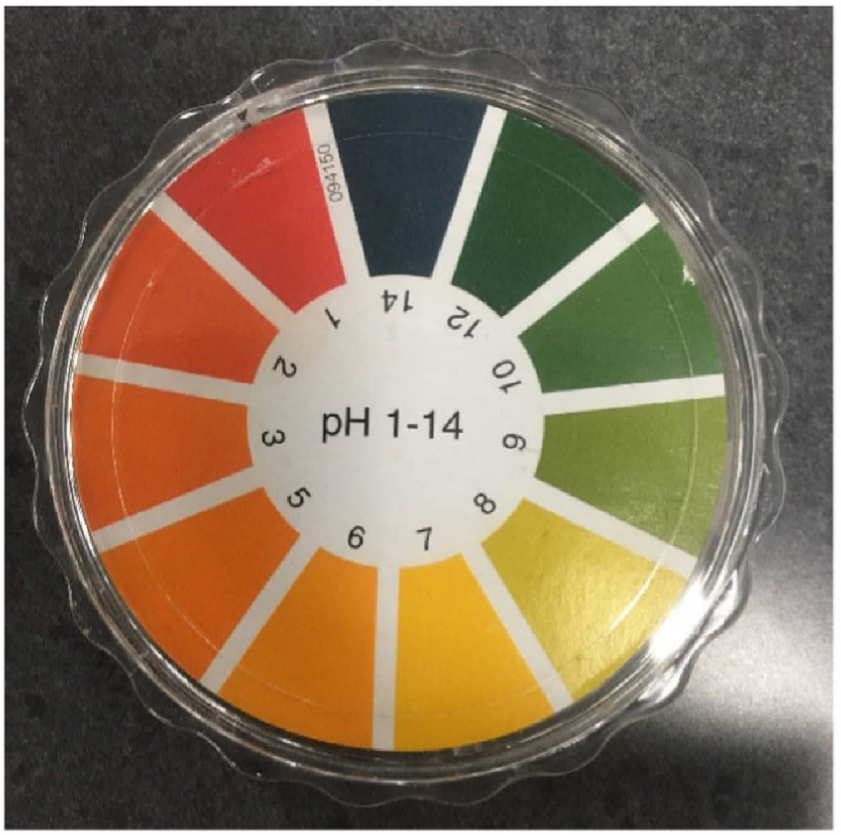

Before air flow

After air flow

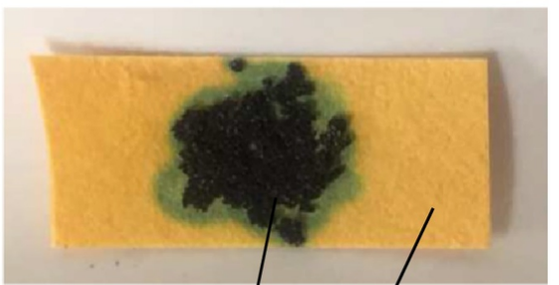

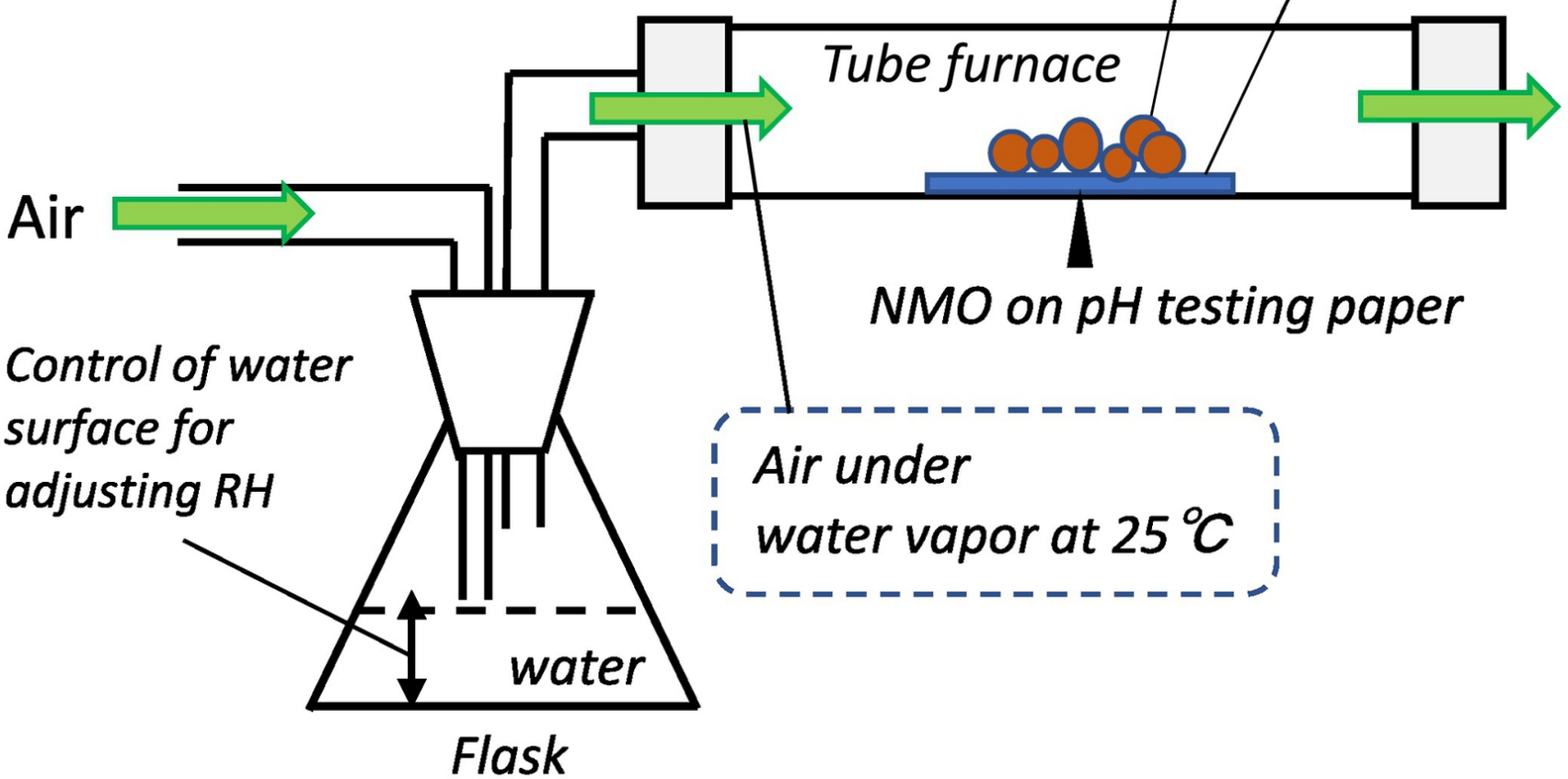

Figure 2

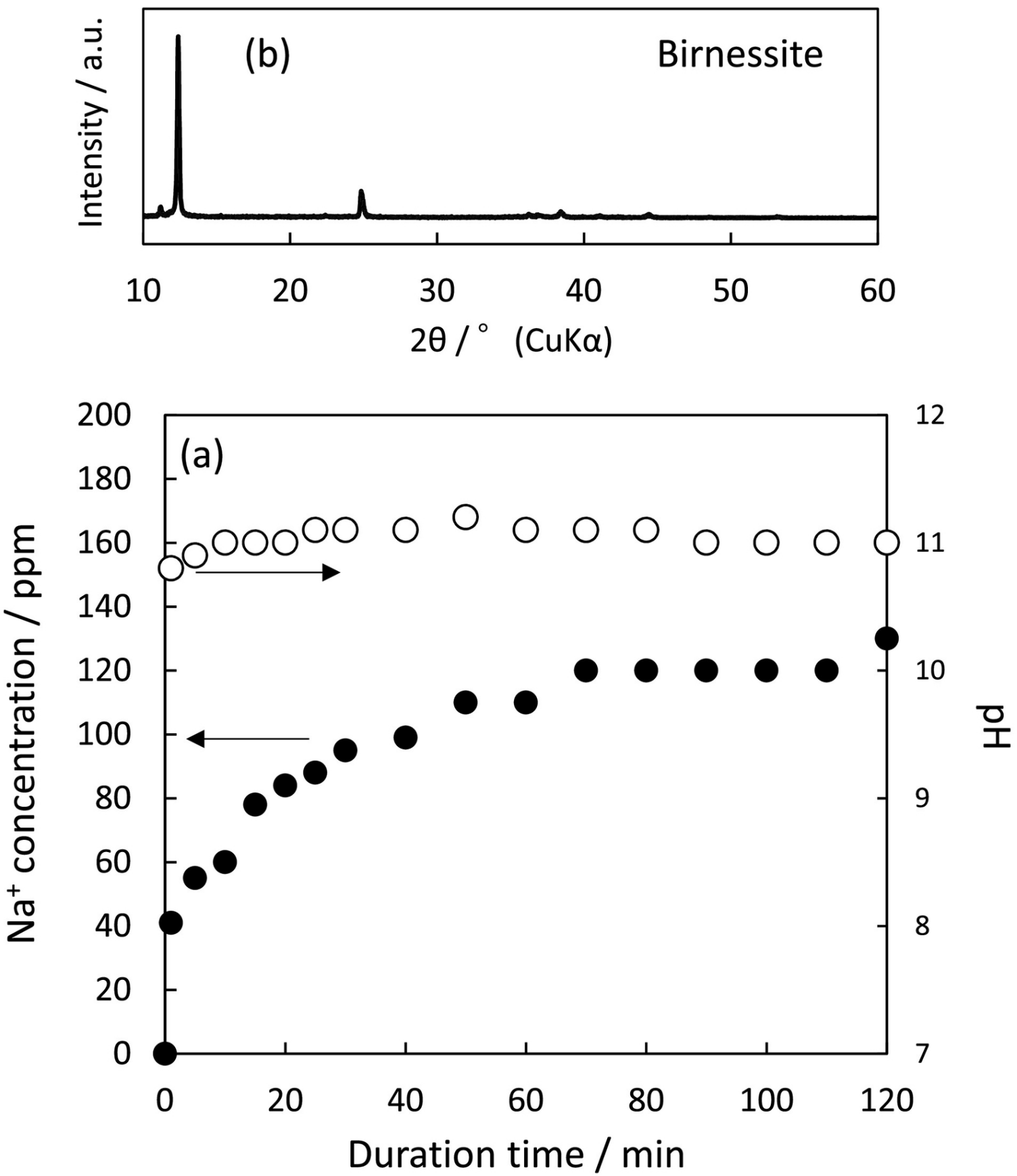
(b)
Birnessite
Intensity / a.u.
10
20
30
40
50
60
2θ / ° (CuKα)
(a)
200
180
160
140
120
100
80
60
40
20
0
12
11
10
9
8
7
pH
Na+ concentration / ppm
0
20
40
60
80
100
120
Duration time / min

Figure 3

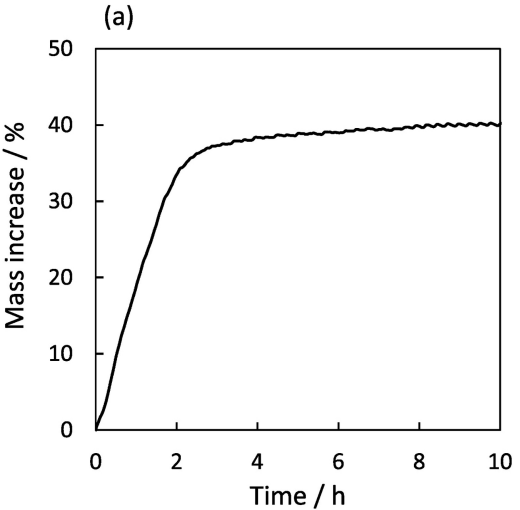
(a)
Mass increase / %
50
40
30
20
10
0
0
2
4
6
8
10
Time / h

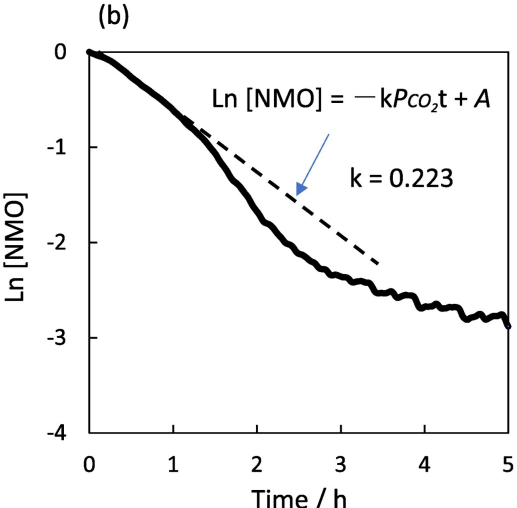
(b)
Ln [NMO] = — kPco_2t + A
k = 0.223
Ln [NMO]
0
-1
-2
-3
-4
0
1
2
3
4
5
Time / h

Figure 4

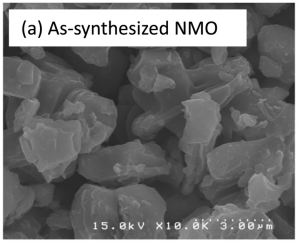
(a) As-synthesized NMO
15.0kV X10.0K 3.00μm

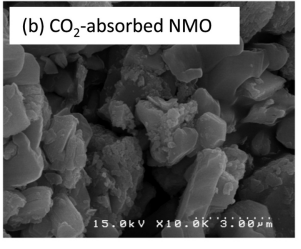
(b) CO_2-absorbed NMO
15.0kV X10.0K 3.00μm

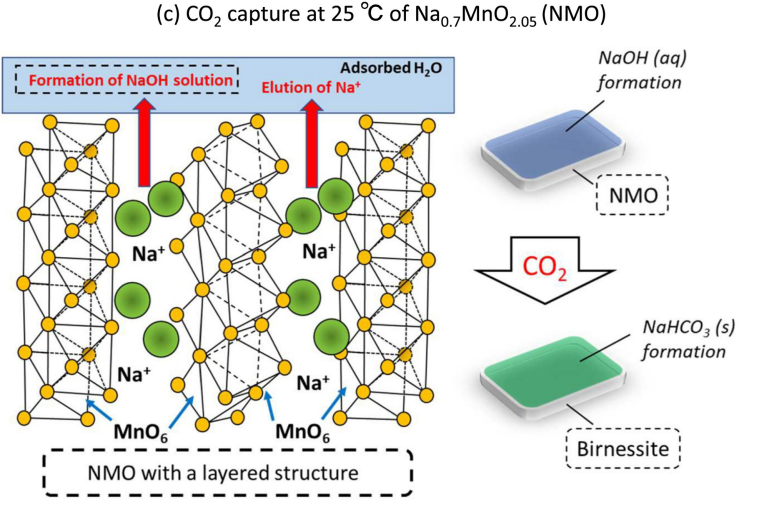
(c) CO_2 capture at 25 ℃ of $Na_{0.7}MnO_{2.05}$ (NMO)
Formation of NaOH solution
Adsorbed H_2O
Elution of Na^+
Na^+
Na^+
Na^+
Na^+
MnO_6
MnO_6
NMO with a layered structure
NaOH (aq) formation
NMO
CO_2
$NaHCO_3$ (s) formation
Birnessite

Figure 5

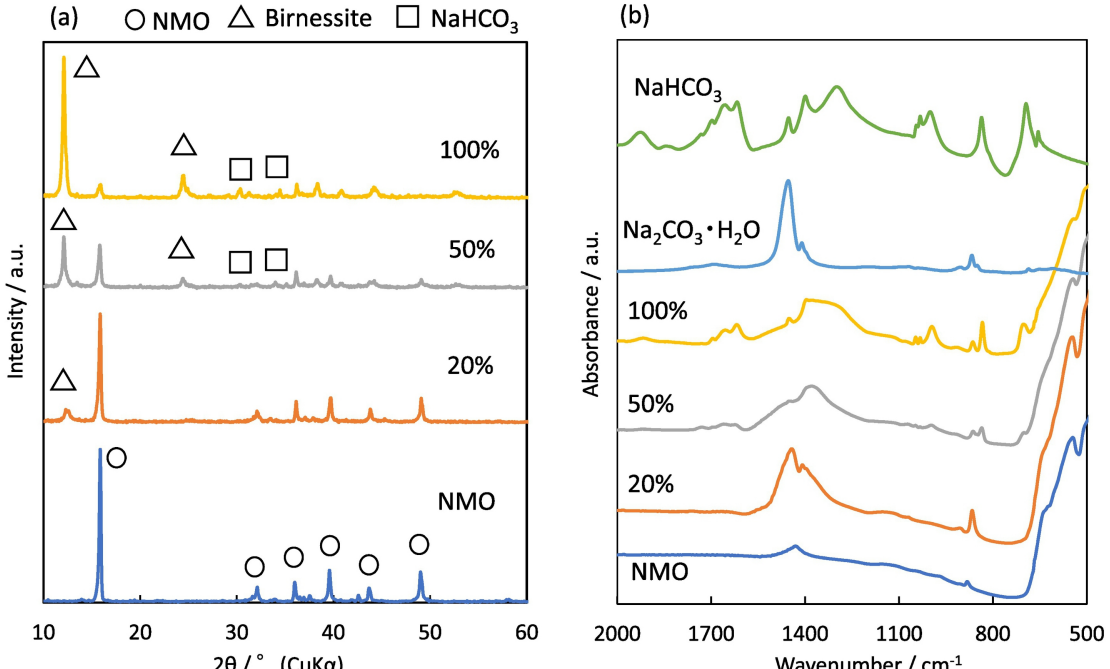
(a)
NMO
Birnessite
NaHCO3
100%
50%
20%
NMO
Intensity / a.u.
10
20
30
40
50
60
2θ / ° (CuKα)
(b)
NaHCO3
Na2CO3・H2O
100%
50%
20%
NMO
Absorbance / a.u.
2000
1700
1400
1100
800
500
Wavenumber / cm-1

Figure 6

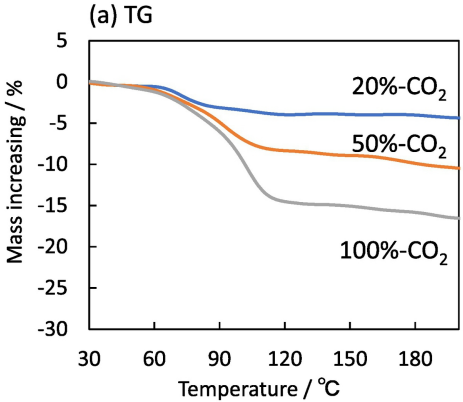

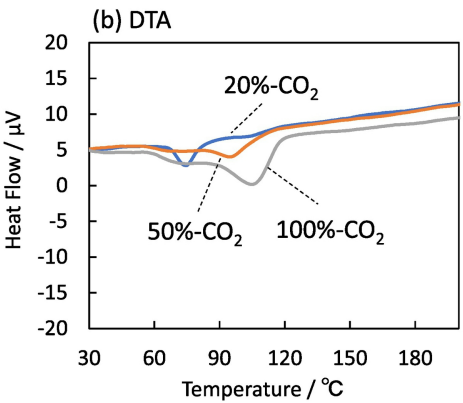

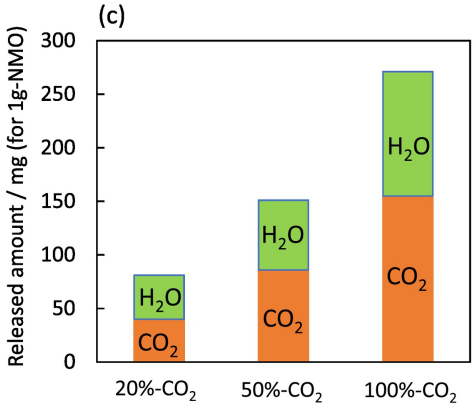

(d)

CO_2 concentration (%)	CO_2 absorption for 1g-NMO (mg)	H_2O absorption for 1g-NMO (mg)
20	40	41
50	86	65
100	155	116

Figure 7

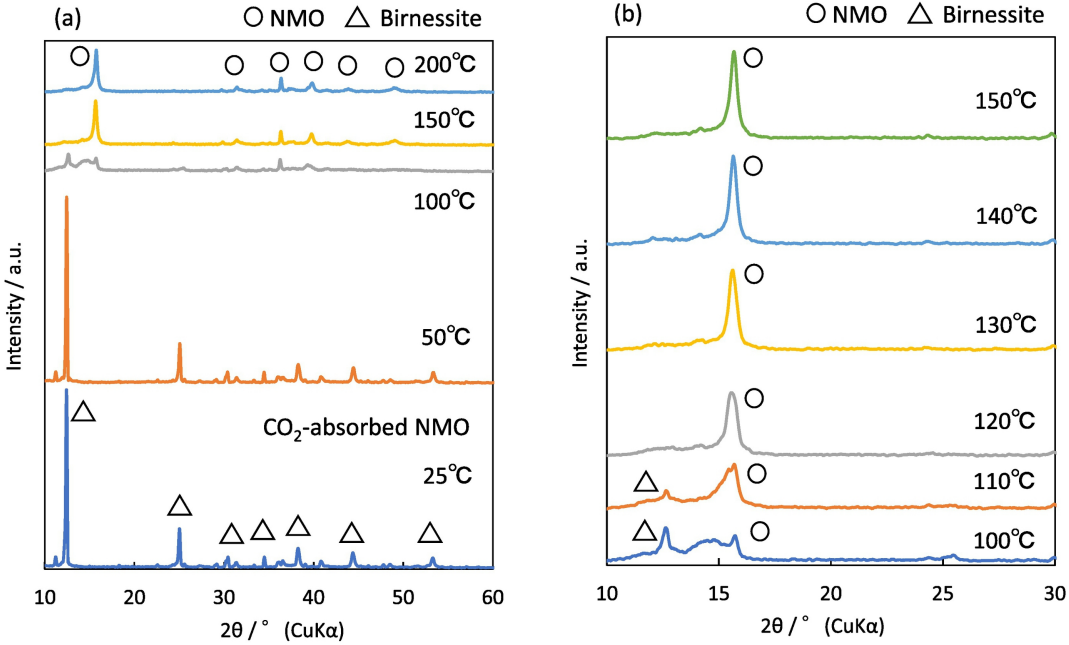
(a)
NMO
Birnessite
200℃
150℃
100℃
50℃
CO2-absorbed NMO
25℃
Intensity / a.u.
10
20
30
40
50
60
2θ / ° (CuKα)
(b)
NMO
Birnessite
150℃
140℃
130℃
120℃
110℃
100℃
Intensity / a.u.
10
15
20
25
30
2θ / ° (CuKα)

Figure 8

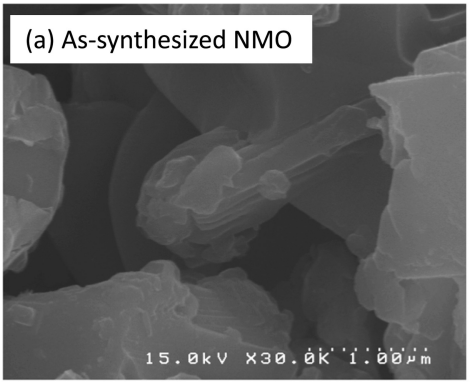
(a) As-synthesized NMO
15.0kV X30.0K 1.00μm

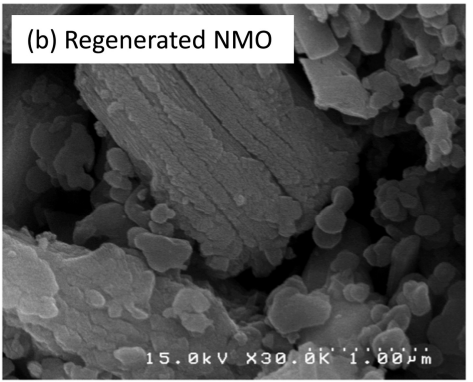
(b) Regenerated NMO
15.0kV X30.0K 1.00μm

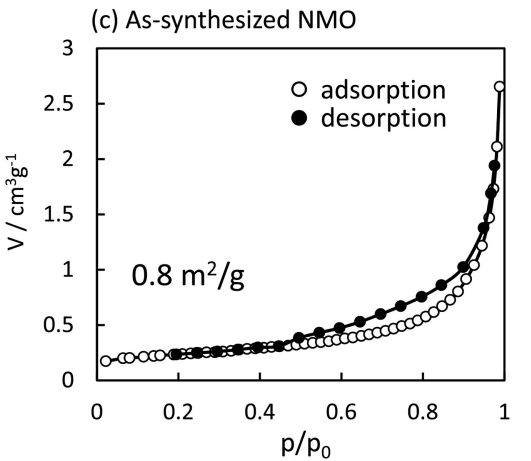
(c) As-synthesized NMO
adsorption
desorption
0.8 m²/g
V / cm³g⁻¹
p/p₀
0
0.5
1
1.5
2
2.5
3
0.2
0.4
0.6
0.8

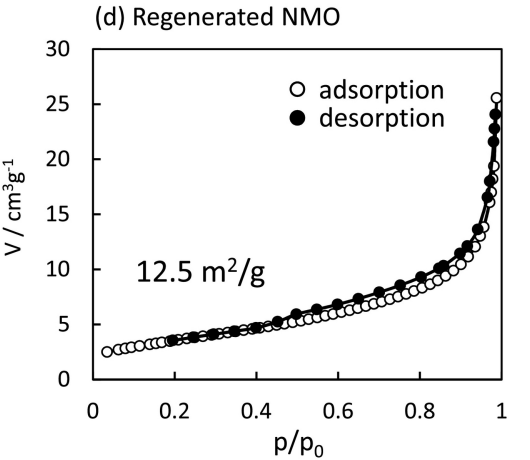
(d) Regenerated NMO
adsorption
desorption
12.5 m²/g
V / cm³g⁻¹
p/p₀
0
5
10
15
20
25
30
0.2
0.4
0.6
0.8
1

Figure 9

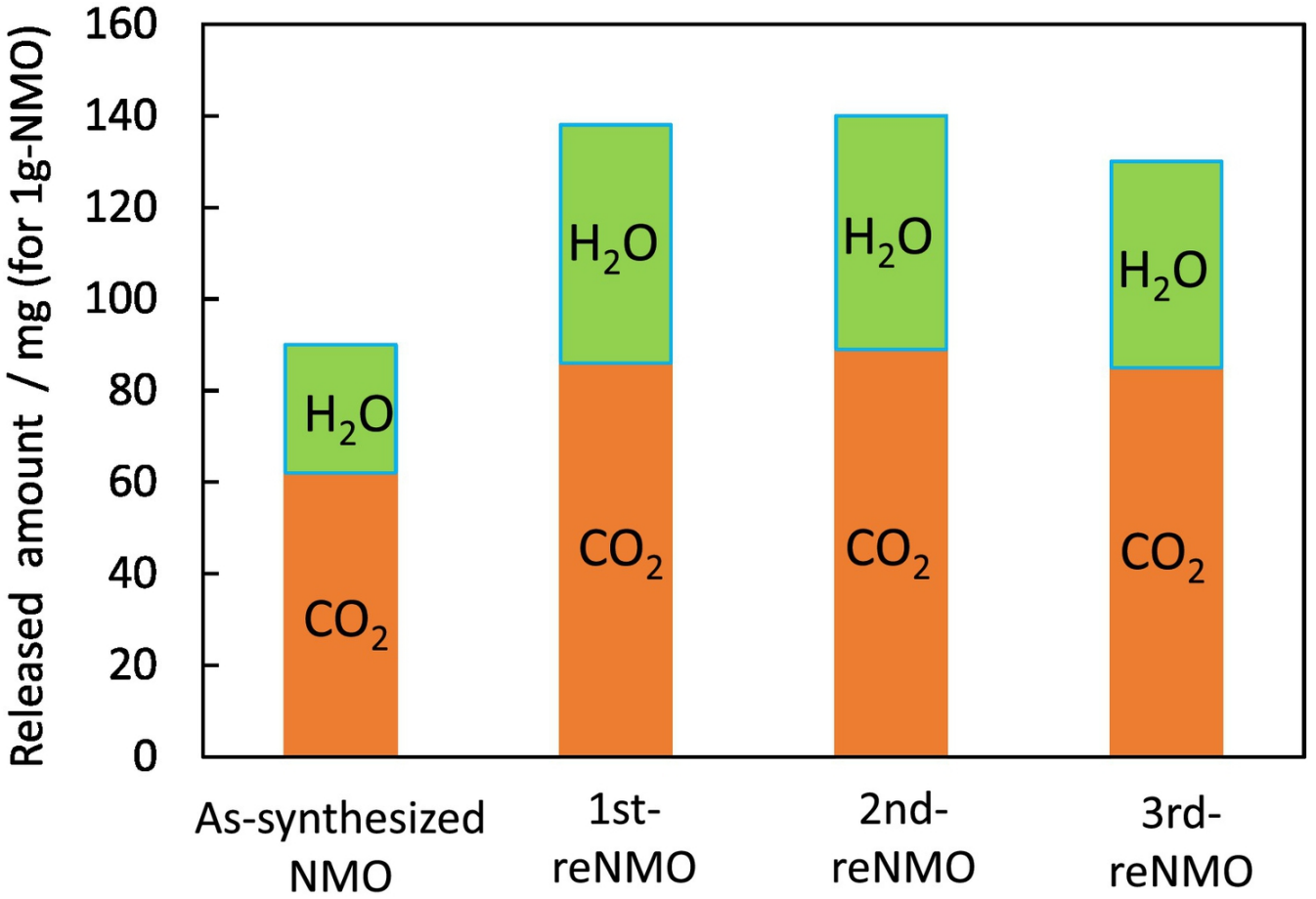

	CO_2 released for 1g-NMO (mg)	H_2O released for 1g-NMO (mg)
As-synthesized NMO	62	28
1st-reNMO	86	52
2nd-reNMO	89	51
3rd-reNMO	85	45

Figure 10